Neuropathology and Applied Neurobiology

WILEY

Neuropathology and Applied Neurobiology
JOURNAL OF THE BRITISH NEUROPATHOLOGICAL SOCIETY

ORIGINAL ARTICLE OPEN ACCESS

Early Regional Microglial Remodelling in the Hippocampus of the *App*$^{NL\text{-}G\text{-}F}$ Alzheimer's Model

Ryan J. Bevan[1] | Jessica F. Minett[2] | Alice L. Smith[1] | Ana Cardus Figueras[1] | Philip R. Taylor[1,3]

[1]UK Dementia Research Institute at Cardiff University, Cardiff University, Cardiff, UK | [2]School of Biosciences, Singelton Campus, Swansea University, Swansea, UK | [3]Systems Immunity Research Institute, Heath Park, Cardiff University, Cardiff, UK

Correspondence: Philip R. Taylor (taylorpr@cardiff.ac.uk)

Received: 26 November 2025 | **Revised:** 24 April 2026 | **Accepted:** 11 May 2026

Keywords: Alzheimer's disease | *App*$^{NL\text{-}G\text{-}F}$ | hippocampus | microglia | microglia morphology

ABSTRACT

Aims: Microglia undergo profound structural and functional changes during Alzheimer's disease, yet the earliest stages of morphological remodelling that occur prior to amyloid deposition remain poorly defined. We hypothesised that microglia in the hippocampus of *App*$^{NL\text{-}G\text{-}F}$ mice would exhibit early, region-specific structural adaptations before local plaque formation, reflecting an initial phase of disease-associated structural remodelling.

Methods: Two-month-old *App*$^{NL\text{-}G\text{-}F}$ and wildtype mice were examined using high-resolution confocal microscopy of Iba1-labelled microglia in the dorsal CA1 apical field. Automated three-dimensional reconstructions were generated in Imaris, and quantitative morphometric analyses quantified cell density, Iba1 coverage, process topology and Sholl-based arbor complexity. Statistical analyses were performed using linear mixed-effects models incorporating sex as a fixed factor in all analyses.

Results: Microglial density and total Iba1 coverage were unaffected in *App*$^{NL\text{-}G\text{-}F}$ mice at this age. In contrast, Sholl analysis revealed significant genotype-dependent reductions in process intersections and total process length, accompanied by reduced individual-cell territorial coverage, indicating an early contraction of the surveillance arbor independent of cell number.

Conclusions: These findings demonstrate that hippocampal microglia in *App*$^{NL\text{-}G\text{-}F}$ mice undergo an early, coordinated structural remodelling before local amyloid deposition becomes apparent. This preplaque adaptation defines an early structural remodelling of hippocampal microglia prior to evident local amyloid deposition, providing new insight into the earliest structural adaptations associated with neuroimmune engagement in AD pathogenesis.

1 | Introduction

Microglia are highly dynamic tissue macrophages that continuously remodel their fine processes to survey the brain parenchyma [1]. Contemporary frameworks position microglia within a multidimensional continuum of context-dependent states shaped by age, sex, regional cues and disease milieu. Their morphology integrates transcriptional, metabolic and environmental inputs rather than reflecting a binary activation state [2, 3]. Morphological features therefore provide an accessible, albeit indirect, window into this adaptive repertoire [4]. However, morphological parameters alone do not directly reflect underlying transcriptional or functional states and must therefore be interpreted as structural correlates rather than definitive indicators of microglial activation. In the healthy brain, such structural plasticity underlies continuous surveillance of neuronal networks, enabling rapid process motility, chemotaxis and transient synaptic engagement [5–7].

Abbreviations: AD, Alzheimer's disease; App, amyloid precursor protein; ARM, activated response microglia; DAM, disease-associated microglia; PCA, principal component analysis.

Summary

- High-resolution 3D morphometry revealed early reductions in microglial arbor complexity and territorial domain in the CA1 region of *App*$^{NL\text{-}G\text{-}F}$ mice.
- Microglial density and parenchymal Iba1 coverage remained preserved, indicating a structural shift independent of cell number.
- These findings define a distinct preplaque microglial phenotype that precedes hippocampal amyloid deposition.

Subtle perturbations, ranging from metabolic stress to the accumulation of misfolded proteins, can elicit measurable structural remodelling. Morphological transitions are best interpreted as indicators of altered microglial engagement with the surrounding tissue, though their temporal relationship to underlying transcriptomic changes remains uncertain [2]. In the mature hippocampus, microglia exhibit highly ramified morphologies characteristic of the postdevelopmental brain [8, 9]. At this stage, the hippocampal microglial network is established, displaying stable density and elaborate arborisation, although sex differences in function have been reported [10, 11]. Reductions in arbor complexity or territory coverage reflect shifts towards surveillance-limited configurations, cytoskeletal reorganisation or metabolic adaptation. Consequently, deviations from this normative architecture can be interpreted as context-dependent remodelling. Defining how such adaptive structural shifts emerge under disease-relevant conditions is central to understanding early immune engagement in neurodegeneration [12, 13].

Alzheimer's disease (AD) offers a particularly relevant framework in which to investigate microglial remodelling. Genetic and imaging evidence place microglia at the centre of AD pathogenesis [14–18]. In advanced disease, microglia accumulate around amyloid plaques, adopting compact, phagocytic morphologies that serve to encapsulate fibrillar Aβ and limit parenchymal toxicity [19]. However, whether such remodelling precedes, parallels or follows amyloid deposition remains unclear. The preplaque phase, marked by rising soluble Aβ and emerging neuronal stress, represents a critical window during which microglia may initiate or amplify neuroimmune cascades [19]. Although morphology alone does not define functional state, it provides a structural correlate of early adaptive changes described transcriptomically in AD [2].

The *App*$^{NL\text{-}G\text{-}F}$ knock-in mouse [20] provides a physiologically relevant model for examining microglial remodelling under native *App* regulation. By introducing three familial AD mutations (Swedish, Iberian and Arctic) into the endogenous locus and maintaining physiologically relevant expression, this model avoids artefacts associated with transgenic overexpression. *App*$^{NL\text{-}G\text{-}F}$ mice develop progressive, Aβ42-biased amyloid pathology and associated cognitive deficits [21]. At early ages (e.g., 2 months), amyloid deposition is detectable in cortical regions but remains minimal in the hippocampus, particularly within the CA1 field [20, 22]. The dorsal CA1 apical field, a region critical for spatial and memory processing, is among the earliest hippocampal sites affected in AD and provides a well-defined domain for quantitative morphological assessment [8, 23]. This regional heterogeneity offers an intrinsic internal control, enabling evaluation of microglial architecture within a plaque-sparse hippocampal territory embedded in an amyloid-positive brain, thereby isolating processes that occur upstream of direct plaque interaction but downstream of systemic amyloidogenic influence.

Microglial morphology encompasses multiple structural dimensions, from somatic distribution to process complexity and territorial organisation. Quantitative morphometric approaches allow these features to be captured in three dimensions, providing a sensitive means of detecting subtle alterations in architecture before overt pathology [24]. Assessing cell density, parenchymal coverage and process topology together offers a multidimensional view of microglial state transitions that aligns with contemporary frameworks of cellular heterogeneity [2]. In the earlier years of microglial research, microglial activation was detected by morphological observation as they transformed from their ramified phenotype in the normal brain to amoeboid morphological appearance in the diseased brain [25]. Although morphology alone cannot define microglial identity, such analyses, applied within a regionally and temporally constrained context, represent a tractable, hypothesis-driven strategy for identifying the earliest manifestations of altered microglial engagement in disease.

Here, we hypothesised that microglia in the dorsal CA1 apical field of *App*$^{NL\text{-}G\text{-}F}$ mice would exhibit measurable, region-specific structural alterations before local amyloid deposition becomes evident. To test this, we applied automated, relatively high-throughput morphometric analysis to quantify microglial density, parenchymal Iba1 coverage and three-dimensional indices of process complexity and territorial organisation. Our findings demonstrate that preplaque hippocampal microglia undergo a coordinated contraction of their arbor, defining an early morphological signature of adaptation to amyloidogenic stress within a plaque-sparse environment.

2 | Materials and Methods

2.1 | Animals

All experimental procedures were approved by the Animal Welfare and Ethical Review Body, a subgroup of the Biological Standards Committee, and conducted in accordance with UK Home Office regulations and the Animal (Scientific Procedures) Act 1986, incorporating EU Directive 2010/63/EU on the protection of animals used for scientific purposes. Experimental cohorts comprised five male and five female wildtype (WT) C57BL/6J mice and four male and four female *App*$^{NL\text{-}G\text{-}F/NL\text{-}G\text{-}F}$ mice (total $n = 18$). The *App*$^{NL\text{-}G\text{-}F}$ knock-in line harbours three familial Alzheimer's disease mutations, Swedish (KM670/671NL), Iberian (I716F) and Arctic (E693G), inserted into the endogenous *App* locus, modelling amyloid-driven pathology under physiological expression. Animals were maintained under specific-pathogen-free conditions with a 12-h light/dark cycle and ad libitum access to food and water. Both sexes were included, and sex was incorporated

as a biological variable in all analyses. Mice were aged to 2 months, corresponding to a preplaque stage in the hippocampal CA1 region.

2.2 | Tissue Preparation

Mice were euthanised via intraperitoneal overdose of Euthatal (Merial Animal Health Ltd.) and perfused transcardially with phosphate-buffered saline (DPBS; Gibco, 14190136). Brains were post-fixed in 1.5% paraformaldehyde (PFA; Sigma, 1.00496) for at least 72 h at 4°C to preserve fine process morphology. Fixed brains were transferred to DPBS containing 0.1% sodium azide (Sigma, S2002) and stored at 4°C until sectioning. Coronal sections (50 μm) were cut on a Leica VT1200S vibratome (Leica Biosystems) and maintained as free-floating sections. Sections corresponding to −1.34 to −2.18 mm relative to bregma were selected using a standard mouse brain atlas to target the dorsal CA1 apical field.

2.3 | Immunofluorescence Staining

Free-floating sections underwent heat-induced epitope retrieval in citrate buffer (Abcam, ab93678) at 95°C for 30 min, followed by permeabilisation in 1% Triton X-100 (Merck, X100) for 5 min. Sections were washed three times in 0.05% Tween-20 in DPBS (Promega, H5152) and blocked for 1 h at room temperature in 5% normal goat serum (Thermo Fisher Scientific). Primary antibody incubation was performed at 4°C for 48 h using rabbit anti-Iba1 (1:2000; FUJIFILM Wako, 019-19741). After washing, sections were incubated with Alexa Fluor 647-conjugated secondary antibody (1:500; Invitrogen, A48285) for 2 h at room temperature. During optimisation, isotype and secondary-only controls were included to confirm antibody specificity. Nuclei were counterstained with DAPI (Invitrogen, D1306), and autofluorescence was quenched with TrueBlack Plus (Biotium, 23014).

For detection of amyloid plaques, brain sections were stained with 10 μM X34 (Sigma, SML1954-5MG), a fluorescent Congo Red derivative that binds β-sheet secondary protein structures, diluted in 40% ethanol (vol/vol) in DPBS containing 20 mM NaOH for 20 min at room temperature [26]. Sections were then washed for 5 min in 40% ethanol (vol/vol) in DPBS with 20 mM NaOH, followed by rehydration in water and PBS. X34 labelled sections were nuclei counterstained with TOPRO-3 (Invitrogen, T3605), and autofluorescence quenched with TrueBlack Plus (Biotium, 23014). Sections were mounted in VECTASHIELD Vibrance (Vector Laboratories, H-1700) and stored at 4°C in the dark until imaging (within 1–2 weeks).

2.4 | Confocal Image Acquisition

Images were acquired on a Leica SP8 Lightning confocal microscope equipped with HyD detectors and LAS X software (v4.3.0). Acquisition parameters were standardised across samples, with laser power and detector gain fixed (10% gain). The CA1 hippocampal region was imaged using a 20× objective (field of view: 581.25 × 581.25 μm; voxel size: 0.284 μm) with two fields captured per animal. Z-stacks spanning 25 μm were collected at 0.5-μm intervals (8-bit depth). Scans were performed at 600 Hz with fivefold line averaging in BrightR mode and 1× optical zoom. Fluorescent channels included DAPI/X34 (405 nm) and Iba1/TOPRO-3 (638 nm), with an additional nonfluorescent channel (488 nm) acquired to monitor residual autofluorescence. Imaging and analysis were performed blind to *App* genotype and pseudo-coloured for visualisation.

2.5 | Morphometric Analysis

All analyses were performed in Imaris (v10.0.1; Bitplane). Raw Leica (.lif) files were converted to .ims format and processed through a standardised batch pipeline. Z-stacks were normalised using the *Normalise Layers* function to correct for depth-related attenuation. The CA1 apical field was manually delineated using the *Surface* tool, and autofluorescent artefacts were excluded by masking a Gaussian-filtered nonfluorescent channel. Images were compiled into a pseudo-time series and normalised with *Normalise Time Points* to ensure comparability across samples. Processed images were exported as TIFFs and reconverted into .ims format using Imaris Converter (v10.0.1).

For segmentation, the DAPI channel was processed using *Linear Stretch* (set to 8) with Gaussian filtering, and the Iba1 channel similarly processed (*Linear Stretch* set to 2). This approach was preferred over *Background Subtraction* or *Threshold Cutoff* as it yielded superior detection of fine microglial processes.

For microglial density and Iba1 coverage, images were projected to 2D using *Project to 2D* (MATLAB XTension). Iba1$^+$ cell bodies were detected with the *Spot* function (diameter = 10 μm; minimum intensity = 5; DAPI intensity sum $\geq 3.5 \times 10^4$). Iba1 coverage was quantified using the *Surface* function (smoothing = 0.1 μm; intensity threshold = 15; minimum surface area = 30 μm^2), and coverage ratios were calculated relative to the delineated CA1 field.

For single-cell morphometrics, 3D datasets were retained. DAPI$^+$ nuclei were segmented (*Surface* tool; smoothing = 0.1 μm; threshold = 5) and filtered by volume (100–800 μm^3) and Iba1 intensity ($> 3 \times 10^4$). Microglia were segmented from the Iba1 channel (threshold = 10; smoothing = 0.05 μm) with inclusion criteria of DAPI overlap > 50 μm^3, volume ratio > 0.2 and exclusion of XY borders < 2 μm. Segmented surfaces were masked and validated manually across representative datasets.

Three-dimensional filament reconstruction was performed with the *Filament Tracer* module. The Iba1 channel was Gaussian smoothed and traced automatically (*Autopath, no spines*) with a starting point diameter of 20 μm and seed threshold of 2.25. Processes were defined as seed points ≥ 10 μm from the soma with a minimum process diameter of 0.2 μm. The *Classify Segments* tool was trained on > 300 positive and 100 negative traces from 10 representative datasets. A maximum connection gap of 5 μm prevented merging of adjacent

cells. All traces were inspected manually with minimal correction where necessary. Sholl intersections were computed at 1-μm radial increments from the soma. Summary statistics were exported using the Batch Statistics function. Territorial field coverage per cell was quantified using the *Convex Hull* (MATLAB XTension).

The final dataset comprised 609 wildtype and 390 $App^{NL\text{-}G\text{-}F}$ microglia (total = 999 cells), representing an average of 55.5 ± 15.5 cells per mouse (mean ± SD). Approximately 2% of cells were excluded during *Convex Hull* analysis, likely due to overlapping territorial boundaries exceeding software constraints.

2.6 | Statistical Analysis

Statistical analyses were conducted in RStudio (v2023.12.1 Build 402) running R (v4.3.1) and Jamovi R interface (v2.5, https://www.jamovi.org). Microglial density, Iba1 coverage and single-cell morphometric parameters (excluding Sholl data) were analysed using linear mixed-effects models (LMMs) with *App* genotype and sex as fixed effects and animal identity as a random intercept. Model residuals were assessed for normality (Shapiro–Wilk test) and homogeneity of variance (Levene's test); log or square root transformations were applied where necessary and this is indicated in the relevant text. Sholl analyses were performed in R using adapted pipelines for LMM of Sholl profiles [27], with intersection counts square root transformed to improve normality. All *p*-values significance was defined as $p < 0.05$, apart from radii-specific interaction *p*-values, which used the significance threshold of $p < 0.01$ due to the number of repeated measures. Data are reported as mean ± SD, except for Sholl profiles (mean ± SEM).

3 | Results

3.1 | Microglial Number and Iba1-Defined Coverage Remain Stable at the Preplaque Stage

In the $App^{NL\text{-}G\text{-}F}$ mouse model, amyloid deposition at 2 months of age manifests as early diffuse focal plaques in the cortex, whereas deposition in the hippocampus, particularly within the CA1 region, has not yet progressed to this stage (representative example, Figure 1a). To assess whether early amyloid pathology influences microglial distribution, Iba1-labelled microglia were quantified in the dorsal hippocampal CA1 region, where overt amyloid deposition is not yet detectable, in wildtype and $App^{NL\text{-}G\text{-}F}$ mice at 2 months of age (Figure 1b). Microglial density was comparable between *App* genotypes (Figure 1c), indicating that overall cell number remains stable at this early stage. Similarly, total Iba1 coverage across the CA1 apical field was unchanged (Figure 1d), suggesting that microglial parenchymal representation is preserved despite emerging amyloid pathology in other brain regions. No effects of sex were apparent from these datasets. These data demonstrate that microglial population density and overall territorial occupancy are maintained within the dorsal CA1 before local plaque deposition. Although total Iba1 coverage reflects population-level parenchymal occupancy across the CA1 field, convex hull analysis and individual tracings capture the spatial domain of individual cells, allowing these measures to distinguish between global coverage and single-cell territorial organisation.

3.2 | Early Simplification of Microglial Arbor Complexity

To determine whether hippocampal microglia exhibit early structural remodelling prior to local amyloid deposition, three-dimensional reconstructions and quantitative Sholl analyses were performed on $Iba1^{+}$ microglia within the dorsal CA1 apical field (Figure 2a). Individual cells were traced using the Imaris Filament Tracer module and manually verified for process continuity. Sholl analysis quantified the number of process intersections at successive radial distances from the soma, providing a distance-resolved measure of arbor complexity. In total, 999 microglia were reconstructed from 18 mice (WT = 10 [5 male and 5 female]; $App^{NL\text{-}G\text{-}F}$ = 8 [4 male and 4 female]), corresponding to an average of 55.5 ± 15.5 (mean ± SD) cells per mouse.

Linear mixed-effects modelling [27], incorporating *App* genotype, sex and their interaction as fixed factors with mouse identity as a random intercept and radius as a repeated measure, revealed a main effect of *App* genotype and a strong *App* genotype-radius interaction, indicating distance-dependent alterations in branching complexity in $App^{NL\text{-}G\text{-}F}$ mice compared to wildtype. A modest three-way interaction with sex was also detected, suggesting subtle sex-dependent modulation of the *App* genotype effect, although no independent main effect of sex was observed.

Consistent with these statistical outcomes, Sholl profiles showed a downward shift in intersection counts, indicating reduced arbor complexity, in $App^{NL\text{-}G\text{-}F}$ microglia relative to wildtype (Figure 2b). When stratified by sex, microglial complexity remained broadly comparable between males and females within each genotype (Figure 2c,d), yet *App* genotype-dependent reductions persisted when analysed within sex (Figure 2e,f). Collectively, these data demonstrate that $App^{NL\text{-}G\text{-}F}$ microglia exhibit an early, distance-dependent simplification of arborisation in the hippocampal CA1, consistent with the onset of morphological adaptation preceding plaque formation.

3.3 | Microglial Morphological Indices

To extend the Sholl-based analysis, additional morphometric parameters were derived from the three-dimensional reconstructions, including total intersections, cumulative process length, total branch points per cell and convex hull volume representing the territorial domain and cell complexity of individual microglia (Figure 3a). Each metric provides a complementary measure of structural elaboration, capturing either local branching behaviour or the overall spatial footprint of single cells.

Linear mixed-effects modelling revealed consistent and significant *App* genotype-dependent reductions across several indices of process complexity. Both total intersections (Figure 3b) and cumulative process length (Figure 3c) were

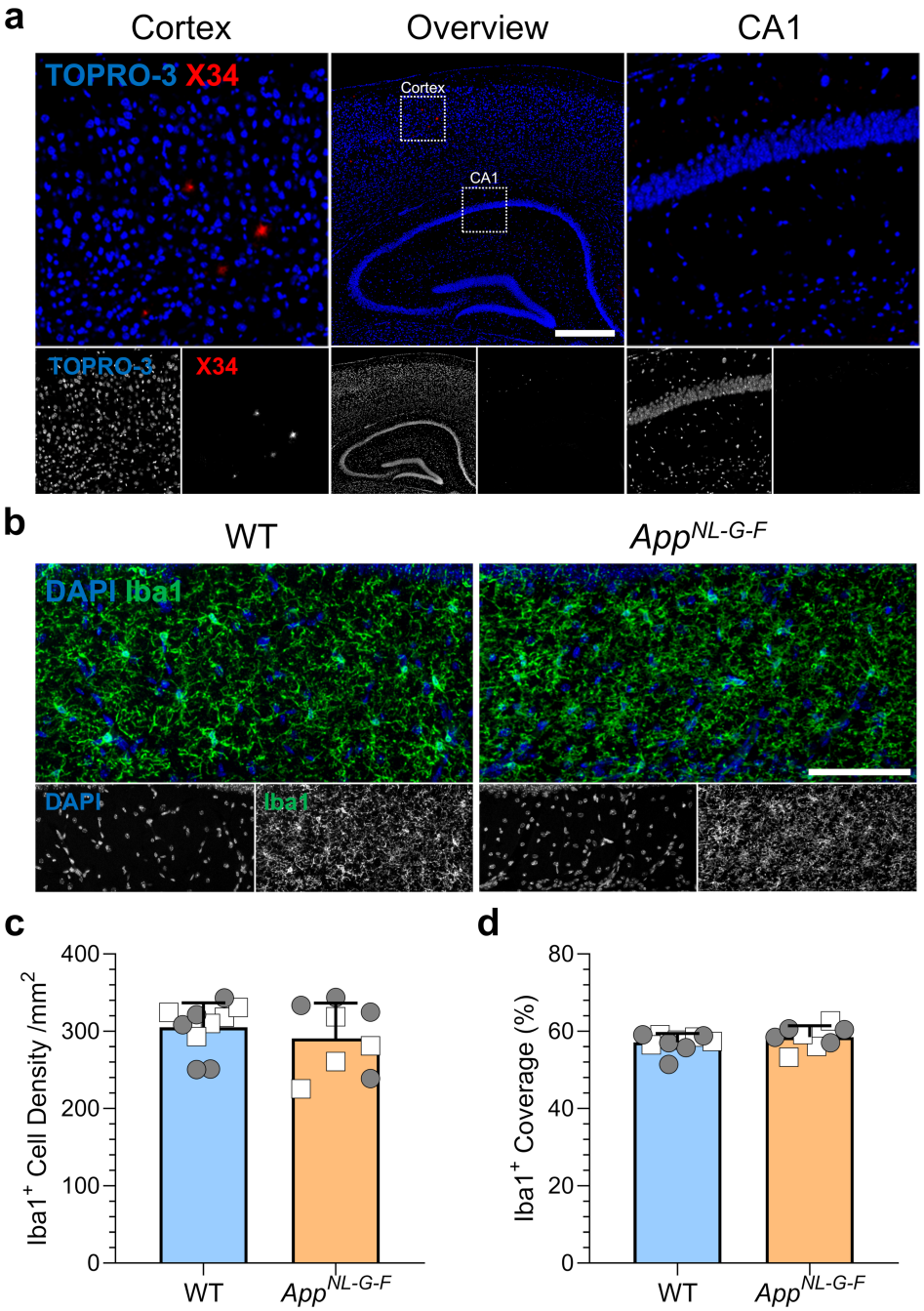

FIGURE 1 | Microglial density and Iba1 coverage are maintained in the dorsal CA1 of 2-month-old $App^{NL\text{-}G\text{-}F}$ mice. (a) Representative example of an $App^{NL\text{-}G\text{-}F}$ cortex and hippocampus at 2 months of age stained with X34 (red) and counterstained with TOPRO-3 (blue), highlighting the presence of amyloid in the cortex and the relative absence of plaque deposition in the CA1 hippocampal region. Scale bar = 500 μm. (b) Representative confocal images showing DAPI (blue) and Iba1 (green) immunofluorescence in the dorsal CA1 apical field of wildtype (WT) and $App^{NL\text{-}G\text{-}F}$ mice. Scale bar = 100 μm. (c,d) Quantification of (c) $Iba1^+$ microglial cell density and (d) Iba1 coverage. All data points represent individual mice (WT = 10 [5 ♂, 5 ♀]; $App^{NL\text{-}G\text{-}F}$ mice = 8 [4 ♂, 4 ♀]); males are indicated by squares and females by circles. Data are summarised as mean ± SD and represent the average of two dorsal CA1 apical hippocampal fields per animal, each encompassing a 0.338-mm^2 field of view (20× objective). Statistical analyses (c,d) were performed using linear mixed-effects models with *App* genotype and sex as fixed factors. (c) Interaction $p = 0.0941$; sex $p = 0.5391$; app genotype $p = 0.3692$. (d) Interaction $p = 0.3019$; sex $p = 0.9695$; app genotype $p = 0.3047$.

reduced in $App^{NL\text{-}G\text{-}F}$ microglia relative to wildtype, independent of sex. Branch point number did not differ significantly between genotypes, although a trend towards a sex-dependent *App* genotype interaction was observed driven by reduced branching in $App^{NL\text{-}G\text{-}F}$ females relative to wildtype counterparts (Figure 3d). Convex hull analysis, a geometrical measure of cell territory coverage, revealed a marked reduction in microglial territorial volume in $App^{NL\text{-}G\text{-}F}$ mice compared with wildtype controls (Figure 3e). These findings suggest that reduced Sholl intersections and process length reflect arbor contraction rather than branch loss, consistent with more compact processes within a smaller surveillance field.

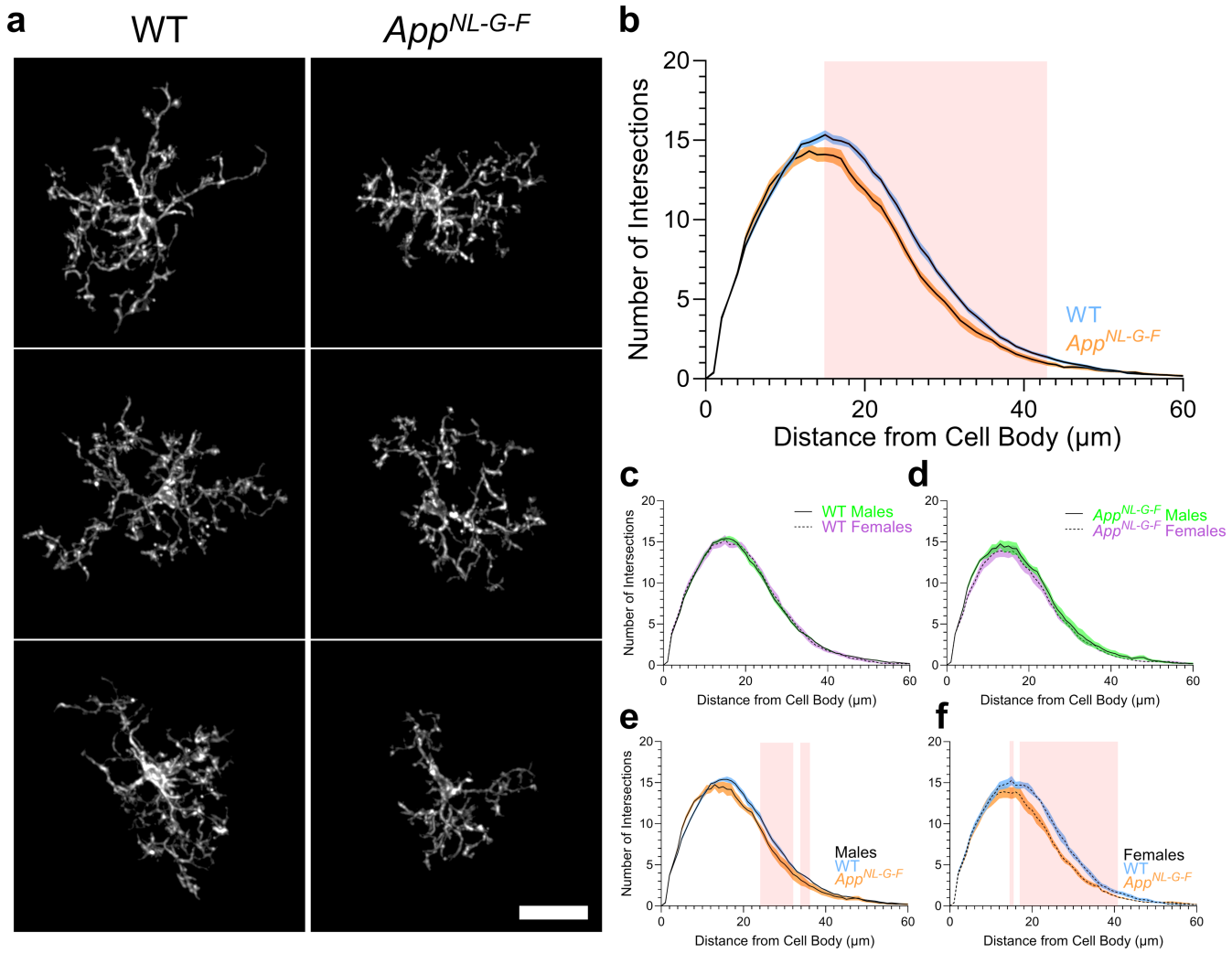

FIGURE 2 | Sholl analysis reveals subtle early alterations in microglial arborisation in the dorsal CA1 of $App^{NL\text{-}G\text{-}F}$ mice. (a) Representative three-dimensional reconstructions of single Iba1$^+$ microglia from the dorsal CA1 apical field of wildtype (WT) and $App^{NL\text{-}G\text{-}F}$ mice, illustrating overall process architecture. Scale bar = 25 μm. (b–f) Quantitative Sholl analyses of microglial arbor complexity across increasing radial distances from the soma. Mean intersection profiles (±SEM) are shown for (b) combined sexes, (c) WT males versus females, (d) $App^{NL\text{-}G\text{-}F}$ males versus females and (e,f) *App* genotype comparisons stratified by sex. Shaded red regions indicate distance intervals showing significant effects derived from linear mixed-effects models. Each data point represents an individual cell traced from the dorsal CA1 apical field. In total, 999 microglia were reconstructed (WT = 10 mice [5 ♂, 5 ♀]; $App^{NL\text{-}G\text{-}F}$ = 8 mice [4 ♂, 4 ♀]; WT males = 70.0 ± 4.8 cells/mouse, WT females = 51.8 ± 13.7, $App^{NL\text{-}G\text{-}F}$ males = 47.2 ± 9.6, $App^{NL\text{-}G\text{-}F}$ females = 50.2 ± 15.5; mean ± SD). Statistical analyses were performed using linear mixed-effects models with *App* genotype, sex and their interaction as fixed factors, radius as a repeated measure and mouse identity as a random intercept. Model outputs revealed significant effects of *App* genotype ($p < 0.0001$) and *App* genotype × radius ($p < 0.0001$), and a modest three-way interaction *App* genotype × radius × sex ($p = 0.0222$), with no independent effect of sex ($p = 0.0887$).

Principal component analysis (PCA) was performed using the above datasets both per-mouse and as single-cells (Figure 3f–h). The PCA plots were able to show divergence between the two genotypes. The first two principal components captured the majority of morphological variance. In the per mouse analysis (Figure 3f), PC1 was dominated by Sholl intersections, process length and territory, representing overall arbor elaboration, whereas PC2 reflected minor variation between territory and branching. In the single-cell PCA (Figure 3g,h), all variables loaded strongly and positively on PC1, again reflecting global complexity, whereas PC2 captured smaller differences in branching and territory. Cell distributions overlapped but were showing early signs of a directional shift between the genotypes. Together, these analyses provide an unbiased confirmation that preplaque microglia in the hippocampal CA1 exhibit a consistent and measurable simplification of their structural processes.

4 | Discussion

Microglia are highly dynamic cells whose morphology integrates transcriptional, metabolic and environmental cues. Here, we demonstrate that microglia within the dorsal CA1 apical field of $App^{NL\text{-}G\text{-}F}$ mice undergo an early, coordinated simplification of process architecture (Figure 2) and a reduction in territorial coverage (Figure 3), while maintaining normal density and overall Iba1 coverage (Figure 1). These findings define an initial

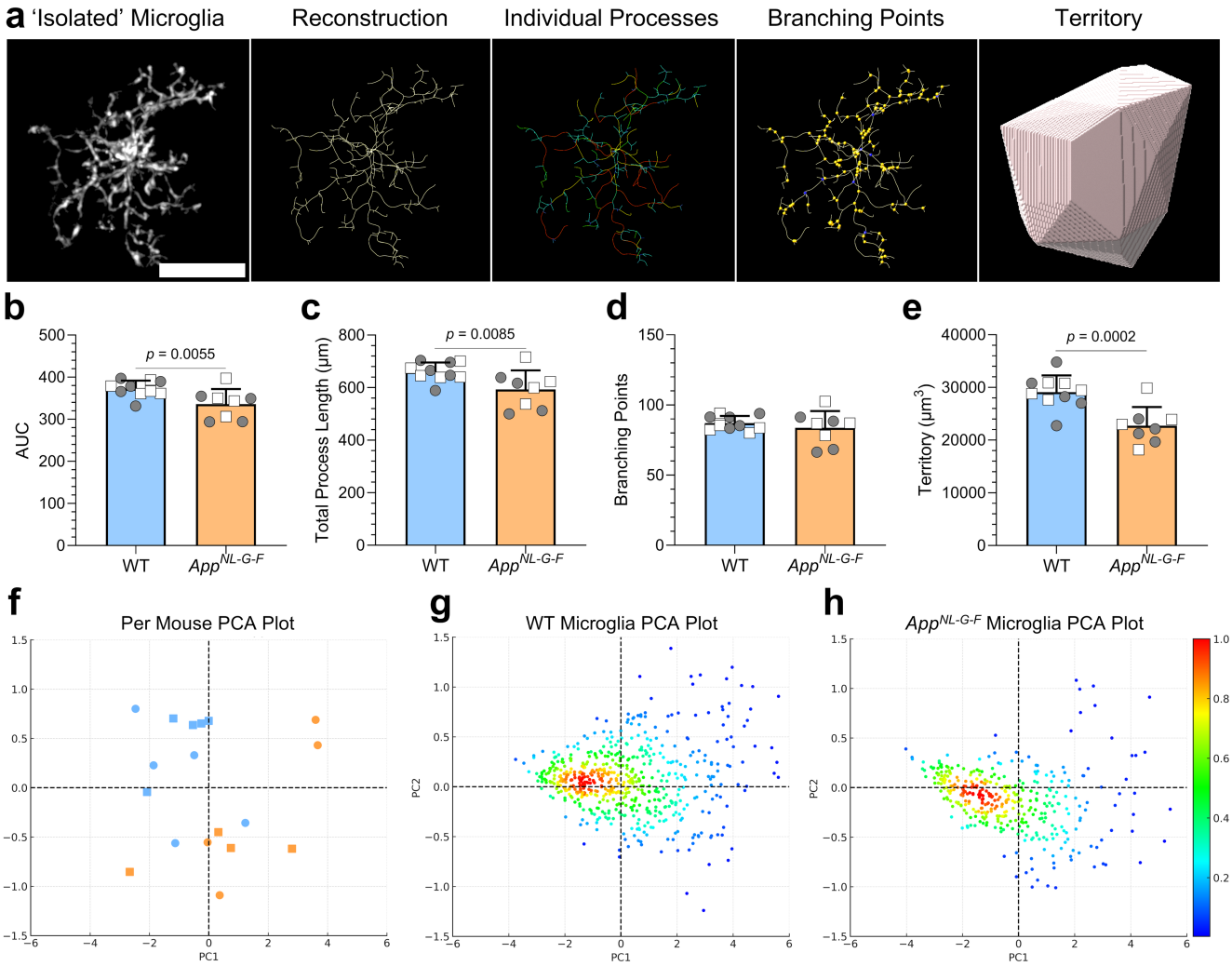

FIGURE 3 | Derived morphometric indices show altered microglial arborisation in *App*$^{NL\text{-}G\text{-}F}$ mice. (a) Representative three-dimensional reconstructions of individual Iba1^{+} microglia from the dorsal CA1 apical field of wildtype (WT) and *App*$^{NL\text{-}G\text{-}F}$ mice, illustrating reduced process elaboration and contracted territorial coverage. Scale bar = 25 µm. (b–e) Quantitative morphometric indices derived from microglia process reconstructions analysis showing (b) total number of intersections (area under sholl curve; AUC), (c) total process length, (d) number of branch points and (e) territory coverage. (f–h) Principal component analysis (PCA) of the microglial morphometric features. (f) Per mouse PCA: each symbol represents one mouse (WT, blue; *App*$^{NL\text{-}G\text{-}F}$, orange); males are squares and females circles. (g,h) Single-cell PCA pseudocolour density maps shown separately for WT (g) and *App*$^{NL\text{-}G\text{-}F}$ (h); colour corresponds to local sample density on a shared scale. Each data point represents a single mouse (mean of reconstructed microglia per animal); bars indicate mean ± SD WT = 10 mice [5 ♂, 5 ♀]; *App*$^{NL\text{-}G\text{-}F}$ = 8 mice [4 ♂, 4 ♀]; WT males = 70.0 ± 4.8 cells/mouse, WT females = 51.8 ± 13.7, *App*$^{NL\text{-}G\text{-}F}$ males = 47.2 ± 9.6, *App*$^{NL\text{-}G\text{-}F}$ females = 50.2 ± 15.5; mean ± SD. Males are indicated by squares and females by circles. Data are summarised as mean ± SD and represent the average of all reconstructed microglia from the dorsal CA1 apical field per animal. Statistical analyses (b–e) were performed using linear mixed-effects models with *App* genotype, sex and their interaction as fixed factors and mouse identity as a random intercept. (b) Interaction $p = 0.1251$; sex $p = 0.1621$; *App* genotype $p = 0.0055$. (c) Interaction $p = 0.1355$; sex $p = 0.1722$; *App* genotype $p = 0.0085$. (d) Interaction $p = 0.0552$; sex $p = 0.2641$; *App* genotype $p = 0.2354$. (e) Interaction $p = 0.3192$; sex $p = 0.1850$; *App* genotype $p = 0.0002$.

and distinct phase of structural remodelling that precedes hippocampal amyloid deposition and is consistent with an adaptive transition in microglial state rather than a loss of homeostatic capacity.

In the mature amyloid-laden brain, microglia undergo marked morphological and molecular transformations in response to plaque deposition. In vivo imaging and histopathological studies consistently show that microglia located near plaques adopt a compact, amoeboid morphology characterised by enlarged somata, thickened primary branches and retracted distal processes. These cells form dense radial clusters around fibrillar Aβ deposits, reminiscent of responses to injury and other insults [19, 28, 29]. This periplaque organisation generates a physical barrier that constrains plaque growth and limits the diffusion of neurotoxic Aβ species [19]. Transcriptionally, plaque-associated microglia reprogram into the 'disease-associated microglia' (DAM) or 'activated response microglia' (ARM) state, marked by upregulation of *Apoe*, *Trem2*, *Clec7a* and lysosomal genes, alongside downregulation of homeostatic markers such as *P2ry12* and *Tmem119* [18, 30]. Collectively, these changes reflect a shift from diffuse parenchymal surveillance to a compact, phagocytic phenotype specialised for amyloid containment.

Our data describe an earlier stage of structural adaptation that precedes amyloid deposition and is mechanistically distinct from the mature, plaque-associated microglial response. The *App*$^{NL\text{-}G\text{-}F}$ knock-in model provides a physiologically relevant context for detecting such changes, as familial AD mutations are introduced into the endogenous *App* locus, preserving native expression and regulation [20]. At 2 months of age, amyloid accumulation is largely confined to cortical regions, whereas the hippocampal CA1 field remains plaque-free, offering an internal comparison between amyloid-exposed and amyloid-naïve territories. Using high-resolution confocal imaging and automated three-dimensional reconstructions, we analysed nearly 1000 individual Iba1$^+$ microglia from a total of 18 mice.

It is important to emphasise that microglial morphology alone does not define transcriptional identity or functional state [2]. Although structural parameters such as process complexity and territorial coverage often correlate with changes in cellular engagement, these measures cannot be assumed to map directly onto specific molecular programmes. Accordingly, the phenotype described here should be interpreted as a well-defined structural state that generates hypotheses regarding underlying biological processes, rather than as direct evidence of mechanism.

Quantitative morphometry revealed a coordinated contraction of process architecture and reduced territorial coverage despite preserved cell density and Iba1 immunoreactivity. Although individual microglia exhibited reduced convex hull-defined territorial domains, total Iba1 coverage across the CA1 field was preserved. These measures capture distinct spatial features: convex hull analysis reflects the surveillance territory of individual cells, whereas Iba1 coverage represents aggregate parenchymal occupancy across the microglial population as a whole. Their divergence is therefore not contradictory but instead indicates preserved overall tissue coverage alongside contraction of single-cell territorial architecture. These findings reveal microglial arbor contraction occurring alongside preserved Iba1$^+$ cell density and overall coverage. This pattern is consistent with a reorganisation of single-cell territorial architecture in the early stages of exposure to an amyloidogenic environment. Both sexes were included, and no sex-dependent differences were detected; however, given increasing evidence for sexual dimorphism in microglial biology [31–33], future studies should interrogate this aspect more directly.

The mechanisms driving this early remodelling are not directly addressed here but may reflect predispositional cues arising during the initiation of amyloidogenesis. Even in the absence of fibrillar plaques, soluble Aβ oligomers, heightened neuronal activity and early metabolic stress can modulate microglial cytoskeletal dynamics and process motility [34]. These changes may be driven by purinergic and TREM2-dependent pathways that govern actin remodelling and energy utilisation [35, 36]. Thus, reduced distal process elaboration may reflect an early adaptive reorganisation of cellular architecture, rather than a degenerative loss of structure. This contracted yet responsive morphology could denote an early transitional state, morphologically distinct from the plaque-engaged phenotype but potentially positioned to respond to diffuse amyloidogenic or neuronal stress signals.

Recent findings suggest that microglia not only respond to amyloid pathology but also participate in its initiation [26]. Microglial depletion in *App*$^{NL\text{-}G\text{-}F}$ mice before plaque onset markedly reduces insoluble Aβ and plaque number, whereas later depletion impairs plaque compaction [26]. This supports a dual-phase framework in which homeostatic microglia seed amyloid aggregates, and reactive microglia subsequently remodel and compact them. Within this model, the early contraction of microglial arbors observed in dorsal CA1 may be compatible with an early phase of amyloid interaction preceding overt plaque deposition. Such structural adaptation may reflect altered microglial engagement with diffuse Aβ species or nascent aggregates, internalising them to generate subthreshold seeds that later nucleate mature plaques. The transition from homeostatic to amyloid-responsive states is increasingly recognised as being orchestrated by TREM2-APOE signalling, which regulates lipid metabolism, phagocytosis and cytoskeletal stability. Our findings therefore provide in vivo structural evidence for an early stage of microglial remodelling that precedes overt plaque deposition and is compatible with proposed frameworks of amyloid interaction.

Although informative, our findings should be interpreted within the context of the following limitations. We used 20× confocal imaging, which enabled large-scale sampling (~1000 cells across 18 mice), though it may lack the resolution required to capture the finest terminal filopodia visible with 63× oil objectives. Likewise, Iba1 immunolabelling, while robust for general morphology, underrepresents the most delicate ramifications contributing to the analysis of the surveillance coverage. Furthermore, microglial processes were reconstructed using the Imaris Filament Tracer module, which used machine learning algorithms for automated process detection. Although this approach ensures high-throughput and objective analysis, some minor mistraced or incomplete processes are inevitable compared to manual traces. Nonetheless, imaging of relatively thick (50 μm) free-floating sections with 25-μm optical depth preserved three-dimensional fidelity, supporting reliable volumetric quantification. Future studies could address this limitation by integrating higher-resolution imaging, multiplexed labelling and live functional assays to directly link these structural signatures with dynamic behaviours such as process motility, phagocytosis and calcium signalling.

The present study focuses on the dorsal CA1 apical field, a region that remains largely plaque-free at this stage despite amyloid deposition elsewhere in the brain [37, 38], providing a controlled context for examining preplaque microglial architecture within an otherwise amyloid-exposed environment. Extending this analysis to additional brain regions with differing temporal profiles of amyloid deposition would be of interest to determine the regional and stage specificity of this phenotype. However, in the *App*$^{NL\text{-}G\text{-}F}$ model, such comparisons are complicated by the intersection of early amyloid deposition with ongoing microglial maturation at younger ages, which may confound interpretation of subtle morphological differences and limit the ability to dissociate disease-related remodelling from developmental effects [39]. Future studies using complementary models or longitudinal approaches will be required to resolve these dynamics.

In conclusion, this study identifies an early, preplaque phase of microglial structural remodelling within the hippocampus of

App$^{NL\text{-}G\text{-}F}$ mice. The observed contraction of arbor complexity and surveillance territory, occurring without changes in density, is consistent with a coordinated reorganisation of microglial architecture that may represent an early adaptive response to amyloidogenic stress. These findings extend current models of AD pathogenesis by highlighting a transitional morphological state that bridges homeostatic surveillance and plaque-associated activation, providing a tractable in vivo framework for probing the earliest microglial responses to amyloidogenic stress.

Author Contributions

Ryan J. Bevan: conceptualization (lead), data curation (lead), formal analysis (lead), investigation (lead), methodology (lead), project administration (supporting), validation (equal), visualisation (lead), writing – original draft (equal), writing – review and editing (equal). **Jessica F. Minett:** formal analysis (supporting), validation (equal), visualisation (supporting), writing – original draft (supporting), writing – review and editing (supporting). **Alice L. Smith:** investigation (supporting), writing – review and editing (supporting). **Ana Cardus Figueras:** investigation (supporting), writing – review and editing (supporting). **Philip R. Taylor:** conceptualization (supporting), funding acquisition (lead), project administration (lead), resources (lead), supervision (lead), validation (equal), visualisation (supporting), writing – original draft (equal), writing – review and editing (equal).

Acknowledgements

We would like to thank the staff of our animal facilities for the care of the animals used in this study.

Funding

This work is supported by the UK Dementia Research Institute (award number UK DRI-3203), which receives its funding from UK DRI Ltd., funded by the UK Medical Research Council, Alzheimer's Society and Alzheimer's Research UK. P.R.T is, in part, funded by the Moondance Foundation.

Ethics Statement

All procedures on mice were approved by the Animal Welfare and Ethical Review Body, a subgroup of the Biological Standards Committee, and conducted in accordance with UK Home Office regulations and the Animal (Scientific Procedures) Act 1986, incorporating EU Directive 2010/63/EU on the protection of animals used for scientific purposes.

Conflicts of Interest

The authors declare no conflicts of interest.

Data Availability Statement

Datasets are available on reasonable request.

Peer Review

For transparency, the peer review documents associated with this article are available at https://doi.org/10.1111/nan.70082.

References

1. A. Nimmerjahn, F. Kirchhoff, and F. Helmchen, "Resting Microglial Cells Are Highly Dynamic Surveillants of Brain Parenchyma In Vivo," *Science* 308, no. 5726 (2005): 1314–1318, https://doi.org/10.1126/science.1110647.

2. R. C. Paolicelli, A. Sierra, B. Stevens, et al., "Microglia States and Nomenclature: A Field at Its Crossroads," *Neuron* 110, no. 21 (2022): 3458–3483, https://doi.org/10.1016/j.neuron.2022.10.020.

3. C. Depp, J. L. Doman, M. Hingerl, J. Xia, and B. Stevens, "Microglia Transcriptional States and Their Functional Significance: Context Drives Diversity," *Immunity* 58, no. 5 (2025): 1052–1067, https://doi.org/10.1016/j.immuni.2025.04.009.

4. J. Reddaway, P. E. Richardson, R. J. Bevan, J. Stoneman, and M. Palombo, "Microglial Morphometric Analysis: So Many Options, so Little Consistency," *Frontiers in Neuroinformatics* 17 (2023): 1211188, https://doi.org/10.3389/fninf.2023.1211188.

5. D. P. Schafer, E. K. Lehrman, A. G. Kautzman, et al., "Microglia Sculpt Postnatal Neural Circuits in an Activity and Complement-Dependent Manner," *Neuron* 74, no. 4 (2012): 691–705, https://doi.org/10.1016/j.neuron.2012.03.026.

6. D. Davalos, J. Grutzendler, G. Yang, et al., "ATP Mediates Rapid Microglial Response to Local Brain Injury In Vivo," *Nature Neuroscience* 8, no. 6 (2005): 752–758, https://doi.org/10.1038/nn1472.

7. H. Wake, A. J. Moorhouse, S. Jinno, S. Kohsaka, and J. Nabekura, "Resting Microglia Directly Monitor the Functional State of Synapses In Vivo and Determine the Fate of Ischemic Terminals," *Journal of Neuroscience* 29, no. 13 (2009): 3974–3980, https://doi.org/10.1523/JNEUROSCI.4363-08.2009.

8. L. J. Lawson, V. H. Perry, P. Dri, and S. Gordon, "Heterogeneity in the Distribution and Morphology of Microglia in the Normal Adult Mouse Brain," *Neuroscience* 39, no. 1 (1990): 151–170, https://doi.org/10.1016/0306-4522(90)90229-w.

9. M.-È. Tremblay, B. Stevens, A. Sierra, H. Wake, A. Bessis, and A. Nimmerjahn, "The Role of Microglia in the Healthy Brain," *Journal of Neuroscience* 31, no. 45 (2011): 16064–16069, https://doi.org/10.1523/JNEUROSCI.4158-11.2011.

10. D. Guneykaya, A. Ivanov, D. P. Hernandez, et al., "Transcriptional and Translational Differences of Microglia From Male and Female Brains," *Cell Reports* 24, no. 10 (2018): 2773–2783.e6, https://doi.org/10.1016/j.celrep.2018.08.001.

11. J. C. Savage, M. Carrier, and M.-È. Tremblay, "Morphology of Microglia Across Contexts of Health and Disease," *Methods in Molecular Biology* 2034 (2019): 13–26, https://doi.org/10.1007/978-1-4939-9658-2_2.

12. Q. Li and B. A. Barres, "Microglia and Macrophages in Brain Homeostasis and Disease," *Nature Reviews. Immunology* 18, no. 4 (2018): 225–242, https://doi.org/10.1038/nri.2017.125.

13. T. R. Hammond, C. Dufort, L. Dissing-Olesen, et al., "Single-Cell RNA Sequencing of Microglia Throughout the Mouse Lifespan and in the Injured Brain Reveals Complex Cell-State Changes," *Immunity* 50, no. 1 (2019): 253–271.e6, https://doi.org/10.1016/j.immuni.2018.11.004.

14. J. C. Lambert, C. A. Ibrahim-Verbaas, D. Harold, et al., "Meta-Analysis of 74,046 Individuals Identifies 11 New Susceptibility Loci for Alzheimer's Disease," *Nature Genetics* 45, no. 12 (2013): 1452–1458, https://doi.org/10.1038/ng.2802.

15. B. W. Kunkle, B. Grenier-Boley, R. Sims, et al., "Genetic Meta-Analysis of Diagnosed Alzheimer's Disease Identifies New Risk Loci and Implicates Aβ, Tau, Immunity and Lipid Processing," *Nature Genetics* 51, no. 3 (2019): 414–430, https://doi.org/10.1038/s41588-019-0358-2.

16. C. Bellenguez, F. Küçükali, I. E. Jansen, et al., "New Insights Into the Genetic Etiology of Alzheimer's Disease and Related Dementias," *Nature Genetics* 54, no. 4 (2022): 412–436, https://doi.org/10.1038/s41588-022-01024-z.

17. R. Sims, S. J. van der Lee, A. C. Naj, et al., "Rare Coding Variants in PLCG2, ABI3, and TREM2 Implicate Microglial-Mediated Innate Immunity in Alzheimer's Disease," *Nature Genetics* 49, no. 9 (2017): 1373–1384, https://doi.org/10.1038/ng.3916.

18. H. Keren-Shaul, A. Spinrad, A. Weiner, et al., "A Unique Microglia Type Associated With Restricting Development of Alzheimer's Disease," *Cell* 169, no. 7 (2017): 1276–1290.e17, https://doi.org/10.1016/j.cell.2017.05.018.

19. C. Condello, P. Yuan, A. Schain, and J. Grutzendler, "Microglia Constitute a Barrier That Prevents Neurotoxic Protofibrillar Aβ42 Hotspots Around Plaques," *Nature Communications* 6 (2015): 6176, https://doi.org/10.1038/ncomms7176.

20. T. Saito, Y. Matsuba, N. Mihira, et al., "Single App Knock-In Mouse Models of Alzheimer's Disease," *Nature Neuroscience* 17, no. 5 (2014): 661–663, https://doi.org/10.1038/nn.3697.

21. A. Masuda, Y. Kobayashi, N. Kogo, T. Saito, T. C. Saido, and S. Itohara, "Cognitive Deficits in Single App Knock-In Mouse Models," *Neurobiology of Learning and Memory* 135 (2016): 73–82, https://doi.org/10.1016/j.nlm.2016.07.001.

22. J. Mehla, S. G. Lacoursiere, V. Lapointe, et al., "Age-Dependent Behavioral and Biochemical Characterization of Single APP Knock-In Mouse (APPNL-G-F/NL-G-F) Model of Alzheimer's Disease," *Neurobiology of Aging* 75 (2019): 25–37, https://doi.org/10.1016/j.neurobiolaging.2018.10.026.

23. H. Braak and E. Braak, "Neuropathological Stageing of Alzheimer-Related Changes," *Acta Neuropathologica* 82, no. 4 (1991): 239–259, https://doi.org/10.1007/BF00308809.

24. G. Colombo, R. J. A. Cubero, L. Kanari, et al., "A Tool for Mapping Microglial Morphology, MorphOMICs, Reveals Brain-Region and Sex-Dependent Phenotypes," *Nature Neuroscience* 25, no. 10 (2022): 1379–1393, https://doi.org/10.1038/s41593-022-01167-6.

25. C. Gao, J. Jiang, Y. Tan, and S. Chen, "Microglia in Neurodegenerative Diseases: Mechanism and Potential Therapeutic Targets," *Signal Transduction and Targeted Therapy* 8, no. 1 (2023): 359, https://doi.org/10.1038/s41392-023-01588-0.

26. N. Baligács, G. Albertini, S. C. Borrie, et al., "Homeostatic Microglia Initially Seed and Activated Microglia Later Reshape Amyloid Plaques in Alzheimer's Disease," *Nature Communications* 15, no. 1 (2024): 10634, https://doi.org/10.1038/s41467-024-54779-w.

27. M. D. Wilson, S. Sethi, P. J. Lein, and K. P. Keil, "Valid Statistical Approaches for Analyzing Sholl Data: Mixed Effects Versus Simple Linear Models," *Journal of Neuroscience Methods* 279 (2017): 33–43, https://doi.org/10.1016/j.jneumeth.2017.01.003.

28. J. K. Hefendehl, J. J. Neher, R. B. Sühs, S. Kohsaka, A. Skodras, and M. Jucker, "Homeostatic and Injury-Induced Microglia Behavior in the Aging Brain," *Aging Cell* 13, no. 1 (2014): 60–69, https://doi.org/10.1111/acel.12149.

29. P. Yuan, C. Condello, C. D. Keene, et al., "TREM2 Haplodeficiency in Mice and Humans Impairs the Microglia Barrier Function Leading to Decreased Amyloid Compaction and Severe Axonal Dystrophy," *Neuron* 90, no. 4 (2016): 724–739, https://doi.org/10.1016/j.neuron.2016.05.003.

30. C. Sala Frigerio, L. Wolfs, N. Fattorelli, et al., "The Major Risk Factors for Alzheimer's Disease: Age, Sex, and Genes Modulate the Microglia Response to aβ Plaques," *Cell Reports* 27, no. 4 (2019): 1293–1306.e6, https://doi.org/10.1016/j.celrep.2019.03.099.

31. M.-V. Guillot-Sestier, A. R. Araiz, V. Mela, et al., "Microglial Metabolism Is a Pivotal Factor in Sexual Dimorphism in Alzheimer's Disease," *Communications Biology* 4, no. 1 (2021): 711, https://doi.org/10.1038/s42003-021-02259-y.

32. M. A. Lynch, "Exploring Sex-Related Differences in Microglia May Be a Game-Changer in Precision Medicine," *Frontiers in Aging Neuroscience* 14 (2022): 868448, https://doi.org/10.3389/fnagi.2022.868448.

33. K. B. Casaletto, E. Nichols, V. Aslanyan, et al., "Sex-Specific Effects of Microglial Activation on Alzheimer's Disease Proteinopathy in Older Adults," *Brain* 145, no. 10 (2022): 3536–3545, https://doi.org/10.1093/brain/awac257.

34. S. Mandrekar, Q. Jiang, C. Y. D. Lee, J. Koenigsknecht-Talboo, D. M. Holtzman, and G. E. Landreth, "Microglia Mediate the Clearance of Soluble Abeta Through Fluid Phase Macropinocytosis," *Journal of Neuroscience* 29, no. 13 (2009): 4252–4262, https://doi.org/10.1523/JNEUROSCI.5572-08.2009.

35. C. Madry, V. Kyrargyri, I. L. Arancibia-Cárcamo, et al., "Microglial Ramification, Surveillance, and Interleukin-1β Release Are Regulated by the Two-Pore Domain K+ Channel THIK-1," *Neuron* 97, no. 2 (2018): 299–312.e6, https://doi.org/10.1016/j.neuron.2017.12.002.

36. T. K. Ulland, W. M. Song, S. C.-C. Huang, et al., "TREM2 Maintains Microglial Metabolic Fitness in Alzheimer's Disease," *Cell* 170, no. 4 (2017): 649–663.e13, https://doi.org/10.1016/j.cell.2017.07.023.

37. T. Manabe and T. Saito, "A Decade Progress in the Phenotyping of AppNL-G-F Knock-In Mouse Model of Alzheimer's Disease," *Neuroscience Research* 220 (2025): 104959, https://doi.org/10.1016/j.neures.2025.104959.

38. D. P. Benitez, S. Jiang, J. Wood, et al., "Knock-In Models Related to Alzheimer's Disease: Synaptic Transmission, Plaques and the Role of Microglia," *Molecular Neurodegeneration* 16, no. 1 (2021): 47, https://doi.org/10.1186/s13024-021-00457-0.

39. X. Wang, K. Li, L. Guo, X. Liu, Y. Guo, and W. Zhang, "The Influence of Changes in Microglia Development on the Plasticity of the Developing Visual Cortex Circuit in Juvenile Mice," *Investigative Ophthalmology & Visual Science* 66, no. 4 (2025): 45, https://doi.org/10.1167/iovs.66.4.45.